Aquarius L-band Microwave Radiometer: Three years of radiometric performance and systematic effects

Jeffrey R. Piepmeier, *Senior Member, IEEE*, and Liang Hong, *Member, IEEE,*
Fernando A. Pellerano, *Senior Member, IEEE*

Abstract - The Aquarius L-band microwave radiometer is a three-beam pushbroom instrument designed to measure sea surface salinity. Results are analyzed for performance and systematic effects over three years of operation. The thermal control system maintains tight temperature stability promoting good gain stability. The gain spectrum exhibits expected orbital variations with $1/f$ noise appearing at longer time periods. The on-board detection and integration scheme coupled with the calibration algorithm produce antenna temperatures with NEDT < 0.16 K for 1.44-s samples. Nonlinearity is characterized before launch and the derived correction is verified with cold-sky calibration data. Finally, long-term drift is discovered in all channels with 1-K amplitude and 100-day time constant. Nonetheless, it is adeptly corrected using an exponential model.

I. INTRODUCTION

Aquarius/Satelite de Aplicaciones Cientificas (SAC)-D, a partnership between the United States' National Aeronautics and Space Administration (NASA) and Argentina's Comisión Nacional de Actividades Espaciales (CONAE), was launched into a 657-km altitude, 6-PM ascending node, sun-synchronous polar orbit from Vandenberg, California, USA on June 10, 2011. Providing the first combined active and passive L-band microwave measurements from space, the Aquarius instrument is designed specifically to measure seasonal and interannual variations of SSS in the open ocean [1][2]. The Aquarius radiometer is a three-beam pushbroom passive microwave sensor measuring the first three Stokes parameters at 1413 MHz with 25-MHz bandwidth. With this design, it operates within the 1400-1427 MHz primary exclusive allocation for passive sensing to avoid severe radio-frequency interference (RFI) and still maintain sensitivity to sea surface salinity. The thermally stabilized radiometer is internally calibrated with reference loads and multiple noise diodes after [3] and [4] to measure the first three Stokes parameters and maintain precise radiometric stability (<0.13 K rms) over the 7-day orbit cycle. Over longer time periods, measurements are externally calibrated using global-averaged expected antenna temperatures or the oceanic vicarious cold-point brightness temperature to support retrieval of sea surface salinity with uncertainty <0.2 psu [5][6]. This paper describes the on-orbit performance of the Aquarius radiometer with emphasis on stability, linearity and observed systematic effects.

II. RADIOMETER THERMAL STABILITY

The radiometer hardware is designed to be thermally stable to promote calibration stability <0.13 K rms/7 days. An instrument block diagram is shown in Fig. 1. A thermal controller maintains tight thermal control of the radiometer front end (RFE) and the radiometer back-end (RBE) to less than 0.1^{o}C peak-to-peak over an orbit. The RFE comprises feed components: correlated noise

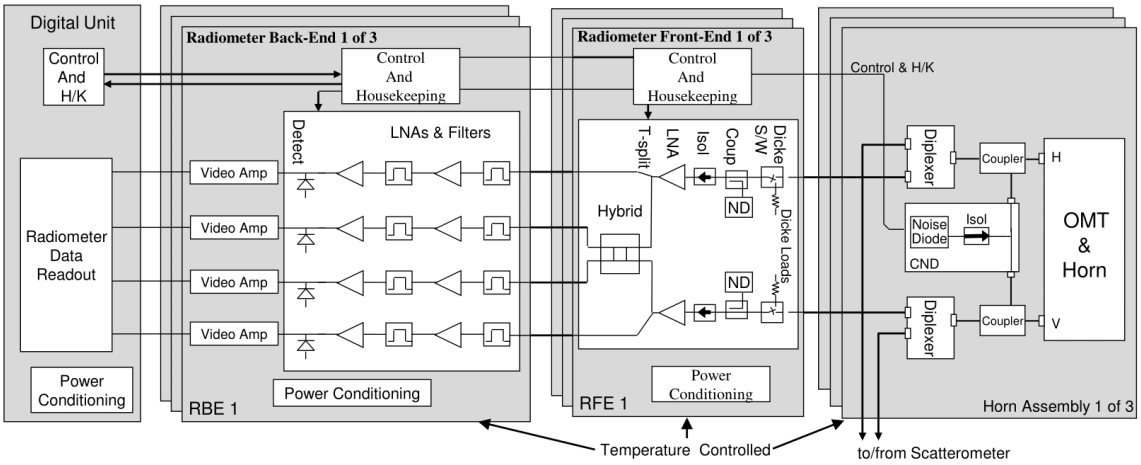

Figure 1. Simplified block diagram showing (from right to left) front-end lossy components, RFE and RBE of each radiometer.

diode (CND), couplers, diplexers, coaxial cables, internal calibration sources (Dicke load DL and noise diode ND) and first stage low-noise amplifiers (LNAs). The RBE comprises the remaining amplifiers, bandpass filters, detectors and voltage-to-frequency converters (VFCs). Front-end lossy components, including ortho-mode transducer (OMT), directional couplers for the external CND, frequency diplexers and connecting coaxial cables lie outside the internal calibration loop and are a potential source of calibration instability. The RFE temperatures are monitored by about a dozen platinum resistance thermometers (PRTs) per beam. Each PRT on front-end components is read every 5.76 s, has <0.01°C resolution, and ±0.5°C accuracy. The Dicke load and internal noise diode temperatures are measured in a bipolar manner to avoid long-term circuit drift.

The temperature history of the instrument (only beam one vertical-polarization denoted 1V is shown as an example; the other channels are similar) is shown in Fig.2 and Fig.3. The temperatures of the front-end lossy components are seen to vary <0.1°C during each orbit and <0.2°C seasonally in Fig. 2(a) and 3(a), respectively. The Dicke load and internal noise diode temperatures are shown in Fig. 2(b) and 3(b) and vary <0.05°C per orbit and <0.1°C annually. Likewise, the detector temperatures in the RBE are shown in Fig. 2(c) and 3(c) and vary 0.05°C and 0.1°C on an orbit and annual basis, respectively.

The Level 2 processing algorithm produces in part calibrated antenna temperatures compensated for physical temperature of the radiometer hardware [13][14]. The demonstrated thermal stability is important for calibration stability. While the ground calibration algorithm corrects the antenna temperature calibration for front-end losses, thermal stability ensures the time-varying systematic error of the correction is negligible. The front-end loss factors were measured in pre-launch testing using techniques similar to [7]. The results are shown in Table I. The total loss factor is 1.3 ± 1% and if left uncompensated would produce a T_A variation of 60 mK seasonally. However, after compensation the uncertainty in the time-varying

portion of the correction is only 5 mK seasonally due to uncertainty in the loss factor estimate. The uncertainty is so low because the hardware is thermally stable.

The long timescale thermal environment promotes calibration stability with low offset error and enables vicarious calibration to compensate scale error. The offset error is negligible by design of a nearly isothermal front-end. The temperature difference between the internal reference load and lossy components is $<2^{o}C$, resulting in a reference temperature bias of <0.2K referred to the feed horn, which is typical of even externally calibrated radiometers [8][9]. The ground calibration algorithm compensates for the gradient. Nonetheless, long-term variation of offset error is not a problem because of the long-term thermal stability shown in Fig. 3.

The active components in the RFE and RBE also go through orbital and seasonal temperature variations shown in Fig. 2(b)-(c) and 3(b)-(c). These variations modulate the radiometer gain, noise figure, calibration noise source, and nonlinearity, all of which were characterized prior to launch. Corrections for temperature dependence in the internal calibration noise source and the nonlinearity are implemented in the ground calibration algorithm. The noise sources have temperature coefficients of approximately 2 ppt, making them more thermally stable than black bodies, at least in the short term. The long-term stability of internal calibration sources is known to suffer problems due to either electronic or passive component changes due to aging or other on-orbit phenomena [10][11]. The gain and offset estimation processes in the calibration algorithm have enough bandwidth to pass orbital thermally driven variations while still averaging down random noise.

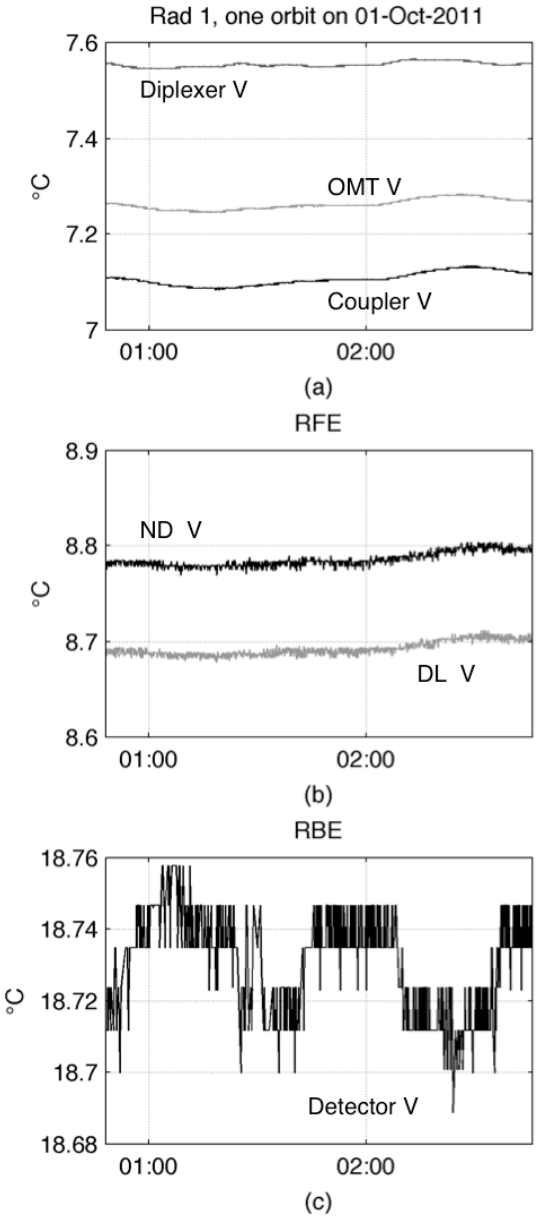

Figure 2. Temperatures of (a) front-end lossy components, (b) internal noise diode and Dicke load, and (c) back-end power detector for radiometer 1 vertical polarization (channel 1V) over an orbit near the beginning of mission on October 1, 2011 at 0100 UTC.

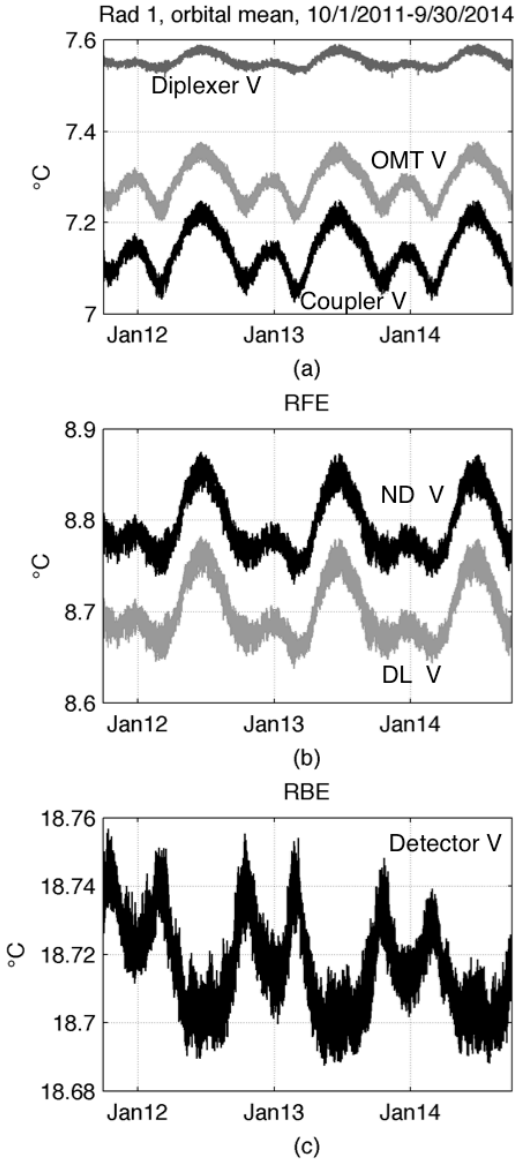

Figure 3. Temperatures of (a) front-end lossy components, (b) internal noise diode and Dicke load, and (c) back-end power detector for beam one vertical polarization (channel 1V) over three years of operation starting October 1, 2011 through September 30, 2014.

TABLE I

LOSS FACTORS FOR FRONT-END COMPONENTS

Loss Factors	Value for 1V
Reflector	1.0003
Feed horn	1.002
Feed throat	1.002
OMT	1.01
Coupler	1.08
Diplexer	1.17
Mismatch	1.01
Product	1.30

III. RANDOM NOISE AND GAIN STABILITY

Of the three beams of the radiometer, the smallest projected beam width on the ground has an along-track distance of 76 km [1]. This distance, coupled with the ground track velocity of 6.8 km s^{-1}, results in an equivalent low-pass filter with a cutoff of 41 mHz. That is, fluctuations in the intensity of naturally occurring thermal emission from Earth will appear at the antenna terminals as a low-pass signal envelope with a time constant of 3.9 s., as shown in the leftmost trace in Fig. 4. The other two beams have along-track footprint widths of 84 and 96 km with equivalent time constants of 4.4 and 5.1 s, respectively. The radiometer hardware, operating scheme, and calibration algorithm are designed to minimize the noise at this timescale.

The radiometer operates synchronously with the scatterometer, whereby the detector readout circuits blank during the transmit pulse and integrate during the radar echo. This integrate and reset operation is repeated every radar pulse repetition interval (PRI). Care is taken in the RF filtering to ensure the radar echo is not detected by the radiometer. Integration is accomplished using a voltage-to-frequency converter (VFC) and digital counters providing boxcar integration equivalent to a 9-ms window with 1-ms reset. The video amplifier must respond to the blanking pulse, drive the VFC with sufficient slew-rate and was implemented with a 14-kHz cutoff frequency. The frequency response curves of the video amplifier (marked RBE) and boxcar integrator (marked PRI) are the two rightmost traces of the plot in Fig. 4. The RBE circuit response has <1% attenuation at the 9-ms period of the integrator.

While further accumulation of the 9-ms samples could be performed on-board up to the antenna's equivalent frequency response, individual samples are downlinked to provide for detection and removal of radio-frequency interference [12]. Some

samples are integrated into pairs to reduce the on-board memory storage requirement, but with no significant impact to the quality of RFI mitigation. The calibration algorithm in the science processing software accumulates multiple samples up to an elapsed time of 1.44 s to produce calibrated antenna temperatures in the Level 2 data product. The Level 2 product still oversamples the antenna response, for the antenna footprint travels only 10 km during in 1.44 s. While the samples are spatially correlated, they remain uncorrelated in noise and are averaged in the Level 3 processing [15].

The 9-ms samples of antenna energy are interspersed by calibration looks of the switched Dicke load and the added noise source to provide periodic gain and offset calibration. A balance is struck between noise equivalent differential temperature (NEDT) degradation due to lost integration time on the antenna and improved calibration noise. Early prototype radiometer test results lead to the Aquarius scheme: 7/12 duty cycle of antenna looks and 5/12 duty cycle of calibration looks [1][3]. In other words, the interleaved calibration and antenna switching during a footprint results in 30% degradation of NEDT over an ideal total power radiometer (neglecting gain instabilities). This is a fine compromise to make because the alternative – grouping calibration looks together within reserved contiguous time like a scanning radiometer – would otherwise result in spatially undersampling the observations of the ocean. The frequency response of the <100% duty cycle integration algorithm is marked by an "L2" for Level-2 data processing in Fig. 4. The spectral sidelobe at 8.3 Hz passes via aliasing the thermal noise responsible for the excess NEDT.

NEDT was characterized before and after launch with results shown in Fig. 5. Before launch, NEDT was estimated by collecting 30 minutes of data to produce 1250 L2-equivalent samples while under tight thermal control and staring at cold-FETs with T_A of approximately 120 K. The long time series was required to obtain low uncertainty in the estimated standard deviation. All channels complied with the required NEDT of 0.16 and 0.22 K for the V and H polarizations and third Stokes

parameter, respectively. After launch, NEDT was measured using a two-sample Allan deviation calculation on data collected over open ocean. Because the conditions are not controlled, only a few hundred samples were obtained. Nonetheless, all the channels demonstrate their compliance with the requirement. The H-pol channels have lower NEDT over ocean because of the lower ocean brightness temperature compared to the cold-FETs used in ground testing.

Because the calibration looks are distributed throughout time, gain and offset coefficient averaging is employed in the algorithm to provide integration time for reducing random noise on their estimates. Frequent calibration also reduces the impact of $1/f$ noise. The normalized power spectrum of radiometer gain is shown in Fig. 6. The response is dominated by orbital thermal fluctuations as evidenced by the strong peak at 5872 seconds or 1 orbit period and at it's second harmonic. There is a slight increase in $1/f$ noise starting at 200 μHz increasing below 100 μHz. To measure the power spectrum down to 10 μHz it was computed using 600,000 noise diode deflections sampled at 1.44-s intervals spanning almost 10 days of operation. The instrument and algorithm provide gain and offset estimates every 1.44 seconds, which are subsequently averaged for additional noise reduction. The offset is averaged for 5 minutes and the gain for 1 minute, which were predetermined using the hardware prototype in ground testing [3]. The frequency responses of the boxcar filters are shown in Fig. 6. As can be seen, the gain and offset averaging filter responses pass the thermally driven and $1/f$ gain variations so the algorithm can produce calibrated antenna temperatures.

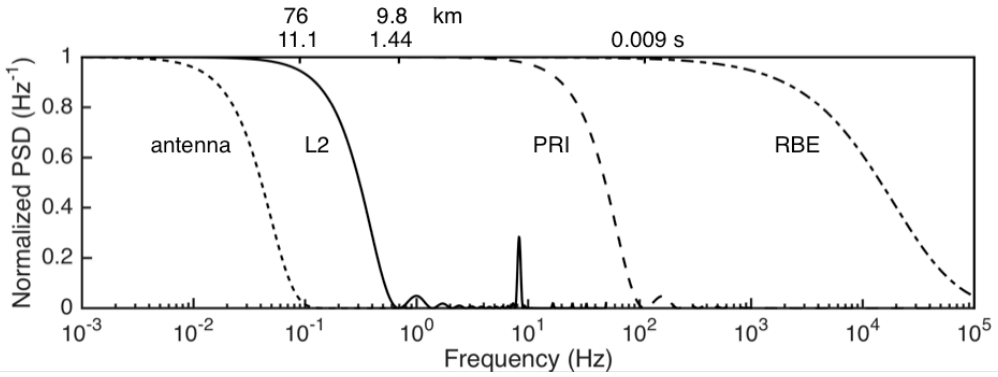

Figure 4. Representative frequency responses of on-orbit and ground averaging performed in radiometer operation and processing. The rightmost two traces show the low pass responses of the internal video amplifier (dash-dot) and the boxcar integrator (dashed), which together produce 9-ms long samples downlinked to the ground. The solid line L2 shows the frequency response of the calibrated antenna temperatures found in the level 2 data product. The dotted line marked antenna shows the equivalent lowpass filter response of the antenna beam one to naturally occurring thermal radiation.

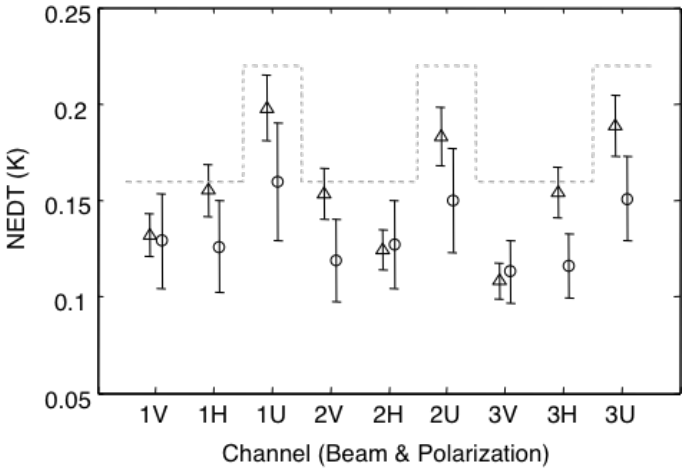

Figure 5. Measured NEDT. Triangles (△) are pre-launch measurement at TA = 100K. Circles (o) are on-orbit estimates made using 2-sample Allan deviation over ocean scenes. Error bars are 3-sigma based on number of samples. Dashed line is the engineering requirement.

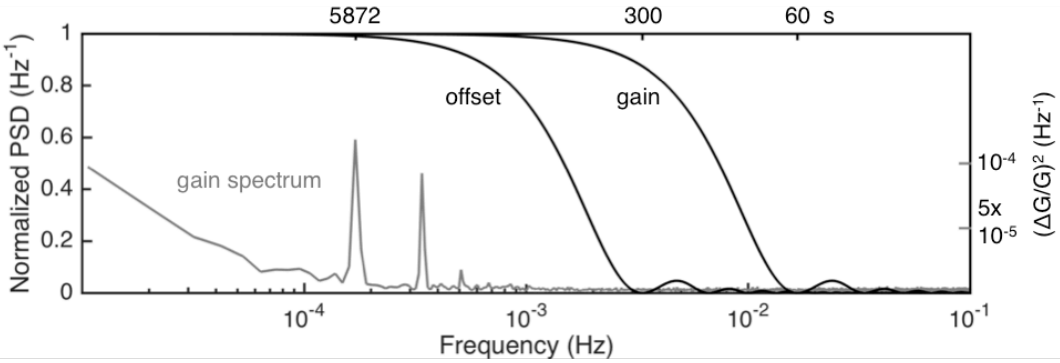

Figure 6. Radiometer gain power spectral density and frequency responses of calibration coefficient averaging filters.

IV. SYSTEMATIC EFFECTS

When known or expected, systematic effects were characterized before launch and provisions for compensation designed into the science operations after launch. Specifically, nonlinearity and noise source drift were found to be sources of error during ground testing. Nonlinearity corrections were derived from ground test data and corrections included in the calibration algorithm. Slow noise source drift with an exponential signature was found in early prototype testing and post-launch calibration was used to correct for drift observed on-orbit. An unexpected systematic effect, however, were nonmonotonic wiggles in the calibration error with a variable quasi-monthly periodicity.

A. Nonlinearity

The radiometer electronics are inherently nonlinear with contributions from microwave amplifiers, power detectors and voltage-to-frequency converters. A physical temperature-dependent correction is derived to apply to the raw counts to force the gain of the radiometer to be constant for all values of antenna temperature counts (see Appendix). During ground testing, noise temperatures between 100 and 3000 K where applied to the radiometer input for different physical temperatures of the RBE, where the last-stage microwave amplifiers and the square-law detectors are located. Fig. 7 shows antenna counts vs. time for one of these tests. During the test, the internal noise sources are triggered to switch the radiometer between antenna and antenna+noise states. The change in radiometer output is called the noise diode deflection, which should be constant for a linear radiometer. The derived correction applied to the raw counts in the calibration algorithm causes the noise diode deflection to remain nearly constant.

The noise diode deflection is conveniently expressed as a deflection ratio (DR) normalized by the deflection at minimum antenna temperature for a test. For a linear radiometer, DR is unity. Fig. 8 shows the DR for beam one horizontal polarization (channel 1H) as a function on antenna counts before and after nonlinearity correction using ground test data. Here we show channel 1H because it has more nonlinearity than 1V. The other Aquarius channels behave in a similar manner. The DR can be interpreted as a gain ratio to predict the maximum error caused by nonlinearity: $\delta T_{max} <$max$|DR-1|\left(T_{A,max}-T_{A,min}\right)$. These ground measurements indicate the algorithm is correcting for up to 1 K of error. To validate the nonlinearity correction after launch, the DR is plotted during a cold-sky calibration (CSC) orbit. There are two main differences between ground calibration and on-orbit validation. On the ground, the minimum antenna temperature used for linearity correction was 100 K, whereas the CSC obtains a mere few kelvins. Also, the ground test ranged up to 3000 K, whereas the on-orbit measurements go to only 300 K. The antenna counts and DR values are plotted in Fig. 9 and Fig. 10, respectively. The CSC data are consistent with the ground test data. Prior to nonlinearity correction the systematic error in antenna temperature over the full dynamic range of the radiometer could be as large as 0.7 K. After correction, the systematic error due to nonlinearity is reduced to below 0.1 K.

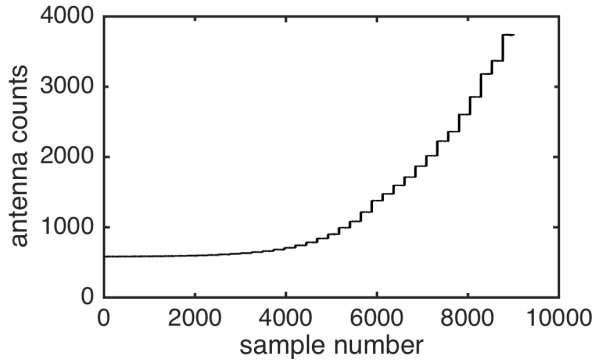

Figure 7. Typical value of antenna counts used for characterizing radiometer nonlinearity. These data were collected using beam one vertical polarization in ground testing. The count values span approximately 100 to 3000 K in antenna temperature.

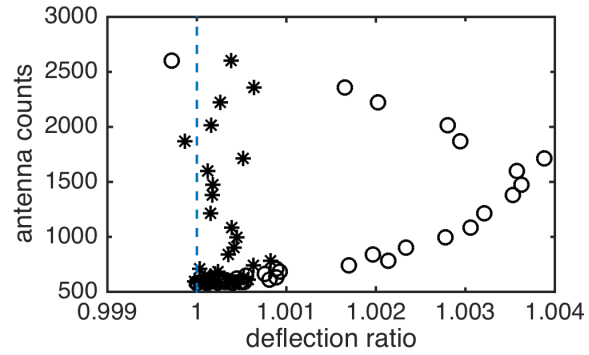

Figure 8. Normalized deflection ratio (DR) before and after application of nonlinearity correction during ground testing, denoted by open circles (o) and asterisks (∗), respectively. The ideal value is unity denoted by the vertical dashed line. Prior to correction, the DR deviates 0.4% over the whole dynamic range of antenna counts (100-3000 K). After correction the residual DR deviation averages 0.05%. These data are typical of the other channels and are from a room temperature test, which is a subset of the data used to characterize the radiometer over physical temperature.

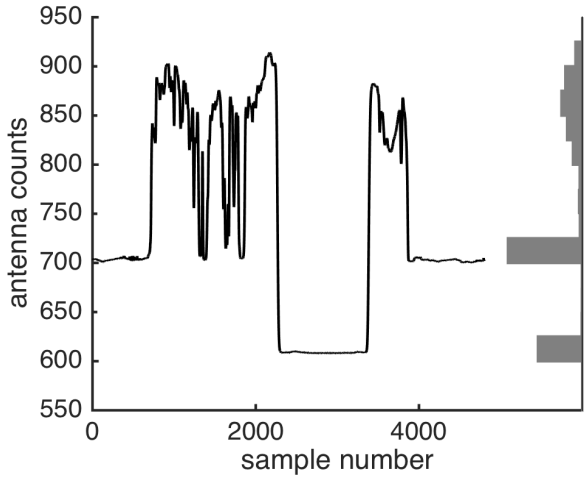

Figure 9. Antenna counts before, during and after a CSC maneuver from 9/22/14. The lowest count value occurs while the antenna views space. A histogram is plotted to the right to show the relative concentration of antenna count values used in the analysis.

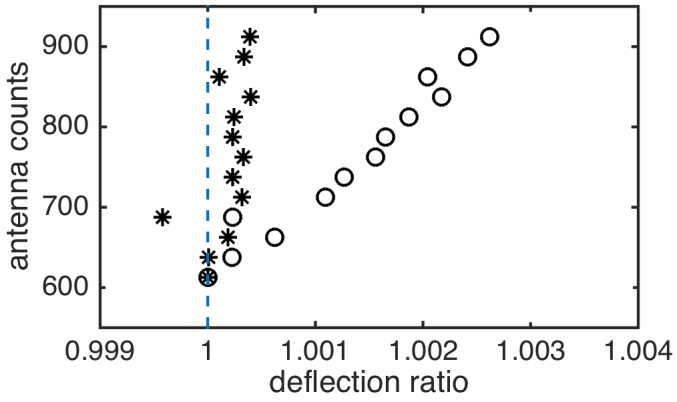

Figure 10. Normalized deflection ratio (DR) before and after application of nonlinearity correction during the CSC maneuver, denoted by open circles (o) and asterisks (∗), respectively. The ideal value is unity denoted by the vertical dashed line. Prior to correction, the DR deviation varies almost 0.3% over the whole dynamic range of antenna counts (radiometrically cold sky to warm land). After correction the residual DR deviation is less than 0.05%.

B. Calibration Drift

Two time-varying systematic effects are evident in long-term analysis of globally-averaged ocean antenna noise temperatures and a model of antenna temperature reported in the level 2 data product. (The model is documented in [13].) There is long-term exponential drift 1 K in amplitude and non-monotonic wiggles 0.1 K in amplitude (see Fig. 11). At the release of version 2 of the L2 data product the effects were determined to be largely assignable to the radiometer hardware, with the drift potentially arising from changes within the RFE or front-end components [16]. At the time, the root cause of the wiggles was undetermined; however, recent work indicates they are caused by voltage-to-frequency converter locking. The main diagnostic technique to determine the source of the effects is analysis of noise diode deflection ratio time series.

Long-term drift in all six radiometer channels is well characterized by an exponential decay. Exponential fits to the calibration model anomaly computed using data through May 19, 2014 are shown in Fig. 11. Their amplitudes and time constants are listed in Table II and range from 0.9 to 1.2 K and from 90 to 110 days, respectively; the consistency amongst channels suggesting some systemic cause to the drift. Note, one kelvin of antenna temperature change over the ocean is equivalent to approximately 0.5% of noise source amplitude change.

If the noise diode added noise temperature T_{ND} is set higher than it should be in the calibration algorithm, the antenna temperature calibration over ocean will be too low. In other words, if the noise diode output decreases over time while the calibration coefficient T_{ND} is held constant in the algorithm, the calibration error over the ocean will drift more negative. This is shown in Fig. 12, which is a graphical version of the simplified calibration equation:

$$T_A = T_{DL} - T_{ND}(C_{DL} - C_A)/(C_{ND} - C_{DL}) \quad (1)$$

where T_x and C_x are the antenna, Dicke load, and noise diode state temperatures and counts for x = A, DL, and ND, respectively. A diagnostic of this effect is the ratio of the internal noise diode deflection above antenna counts (NDA) to the external correlated noise diode deflection above antenna counts (CND) while viewing the ocean. The time series of this NDA/CND ratio initialized to unity for all six radiometer channels are plotted in Fig. 13 and their time constants are listed in the rightmost column on Table II. If the CNDs are assumed to have a different time constant than the internal noise diodes, then the time constant of the ratio is $1/\tau = 1/\tau_{\mathrm{ND}} - 1/\tau_{\mathrm{CND}}$. Prescribing the calibration drift shown in Fig. 11 to the internal noise diode results in CND time constants ranging from 55 to 65 days. This result is consistent with early attempts to calibrate the radiometer gain using the CND instead of the internal noise diode. The drift was reduced but not eliminated. The amplitude of the NDA/CND ratio ranges from 0.4% to 0.6%, which is consistent with the observed drift of 1 K in the calibration model anomaly.

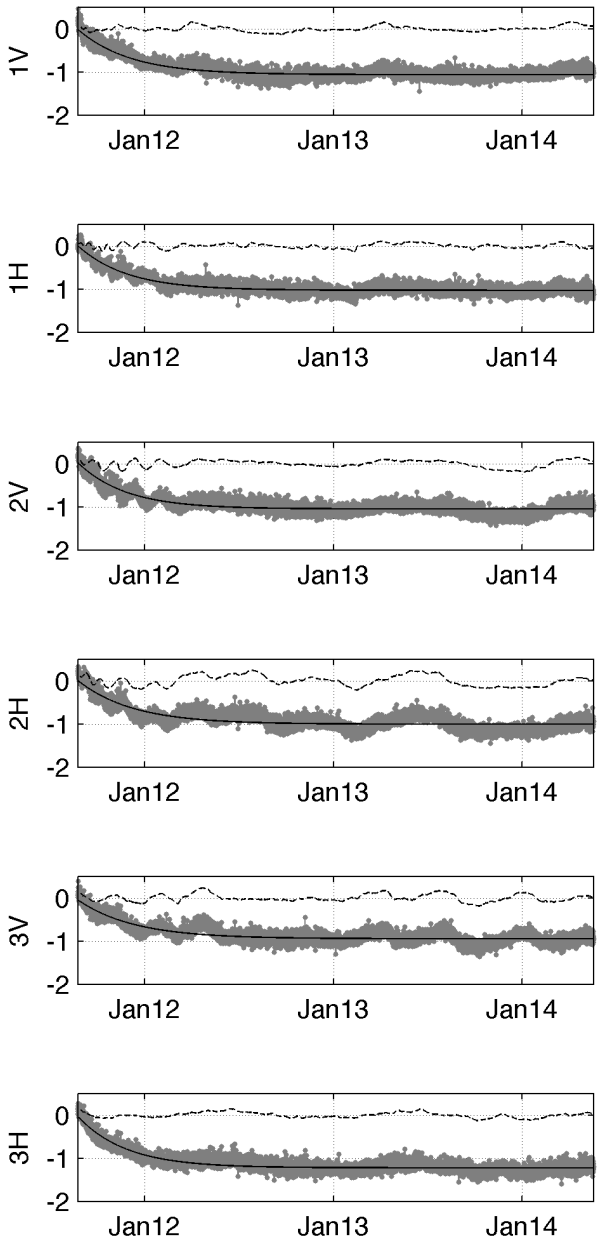

Figure 11. Antenna temperature biases (defined as measured minus modeled averaged every orbit over the global ocean) of all channels (gray lines) exhibit exponential drift (solid lines) from beginning of the mission. Steeper slopes are seen in the first year of mission, with antenna temperature dropping by 1K. After applying an exponential correction to the noise diode added noise temperature, the gain drift is fully compensated with near flat slope (dotted lines).

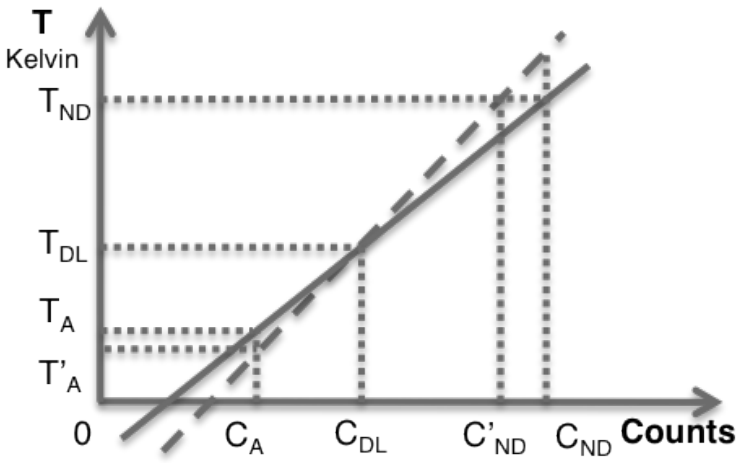

Figure 12. Schematic of calibration error caused by misassignment of noise diode added noise temperature. Solid line is the correct calibration line. Dotted line shows how noise source drift effects calibration error.

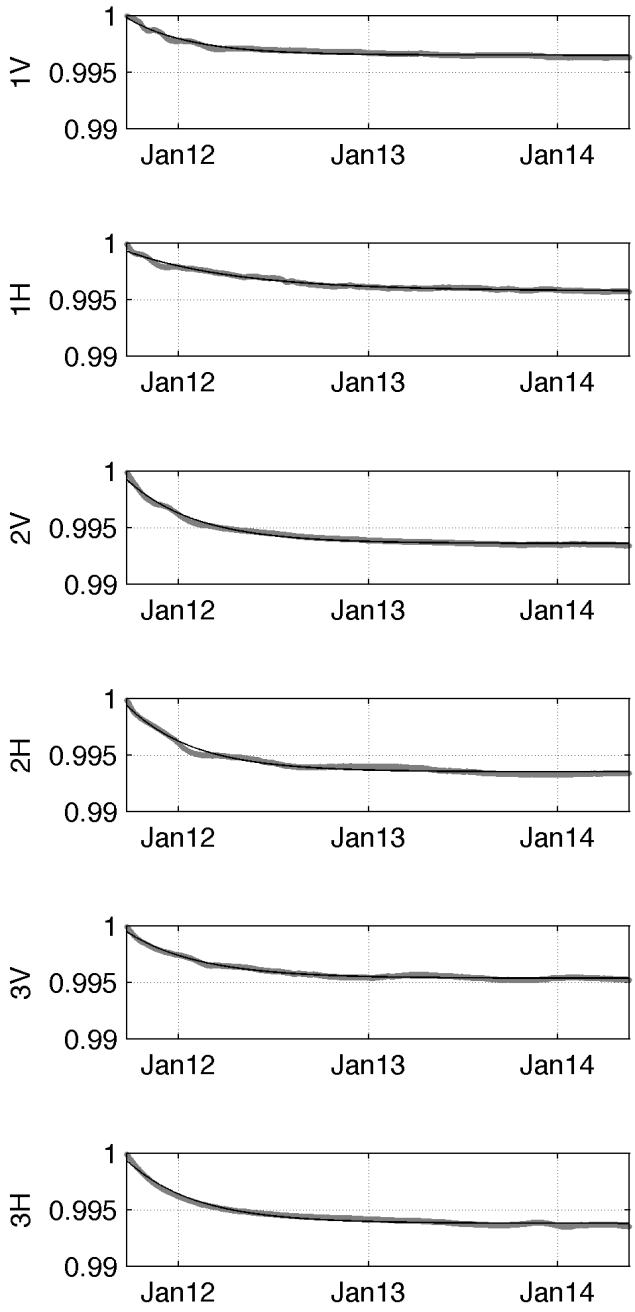

Figure 13. Normalized NDA/CND deflection ratio time series for all six radiometer channels. These DR plots show very similar drift pattern as seen in the calibration drift shown in Fig. 11.

TABLE II

OBSERVED CALIBRATION DRIFT PARAMETERS

Channel	$T_A \sim A\exp(-t/\tau)$		NDA/ CND
	A (K)	τ (days)	τ (days)
1V	1.05	101	122
1H	1.03	95	215
2V	1.07	92	135
2H	1.01	106	130
3V	0.90	109	141
3H	1.19	93	132

V. DISCUSSION

Aquarius microwave radiometer performance and systematic effects were elucidated over three years of operation. All six radiometer channels were found to exhibit a long-term drift, which was well modeled using an exponential decay with 1 K amplitude and 100 day time constant. Nonlinearity corrections derived in ground testing were verified using on-orbit data. Additionally, NEDT measured on-orbit were consistent with pre-launch measurements and meet requirements with margin. The radiometer gain stability characterized using 10 days of data displayed expected orbital fluctuations. It's $1/f$ noise is low enough to allow on-board and calibration algorithm averaging. The radiometer performance is supported by excellent thermal stability via the automatic temperature controller, which limits orbit and inter-seasonal variations to $<0.2^{o}$C. Thus, the radiometer performance is sufficient to enable sea surface salinity retrievals for the Aquarius/SAC-D mission.

REFERENCES

[1] D.M. Le Vine, G.S.E. Lagerloef, F.R. Colomb, S.H. Yueh and F.A. Pellerano, "Aquarius: An Instrument to Monitor Sea Surface Salinity From Space," *IEEE Trans. Geosci. Remote Sens.,* vol.45, no.7, pp.2040–2050, July 2007. http://dx.doi.org/10.1109/TGRS.2007.898092

[2] G. Lagerloef *et al.*, "The Aquarius/SAC-D mission: Designed to meet the salinity remote sensing challenge," *Oceanography*, vol. 21, no. 1, pp. 68–81, Mar. 2008. http://dx.doi.org/10.5670/oceanog.2008.68

[3] A.B. Tanner, W.J. Wilson and F.A. Pellerano, "Development of a high stability L-band radiometer for ocean salinity measurements," *Geoscience and Remote Sensing Symposium, 2003. IGARSS '03. Proceedings. 2003 IEEE International* , vol.2, no., pp.1238–1240 vol.2, 21-25 July 2003. http://dx.doi.org/10.1109/IGARSS.2003.1294069

[4] J.R. Piepmeier, "Calibration of passive microwave polarimeters that use hybrid coupler-based correlators," *IEEE Trans. Geosci. Remote Sens.,* vol.42, no.2, pp.391–400, Feb. 2004. http://dx.doi.org/10.1109/TGRS.2003.817792

[5] D.M. Le Vine, E.P. Dinnat, S. Abraham, P. de Matthaeis, and F.J. Wentz, "The Aquarius Simulator and Cold-Sky Calibration," *IEEE Trans. Geosci. Remote Sens.,* vol.49, no.9, pp.3198–3210, Sept. 2011. http://dx.doi.org/10.1109/TGRS.2011.2161481

[6] C.S. Ruf, "Vicarious Calibration of an Ocean Salinity Radiometer from Low Earth Orbit," *J. Atmos. Oceanic Tech.*, 20(11), pp. 1656–1670, 2003.

[7] C.S. Ruf, S.J. Keihm and M.A. Janssen, “TOPEX/POSEIDON microwave radiometer (TMR): I. Instrument description and antenna temperature calibration,” *IEEE Trans. Geosci. Remote Sens.,* vol. 33, pp. 125–137, Jan. 1995.

[8] E.M. Twarog, W.E. Purdy, P.W. Gaiser, K.H. Cheung and B.E. Kelm, "WindSat on-orbit warm load calibration," *IEEE Trans. Geosci. Remote Sens.,* vol.44, no.3, pp.516–529, March 2006. http://dx.doi.org/10.1109/TGRS.2005.863300

[9] D.B. Kunkee, S.D. Swadley, G.A. Poe, Ye Hong and M.F. Werner, "Special Sensor Microwave Imager Sounder (SSMIS) Radiometric Calibration Anomalies—Part I: Identification and Characterization," *IIEEE Trans. Geosci. Remote Sens.,* vol.46, no.4, pp.1017–1033, April 2008. http://dx.doi.org/10.1109/TGRS.2008.917213

[10] Ruf, C.S., "Characterization and correction of a drift in calibration of the TOPEX microwave radiometer," *IEEE Trans. Geosci. Remote Sens.,* vol.40, no.2, pp.509–511, Feb 2002. http://dx.doi.org/10.1109/36.992824

[11] Brown, S.T., S. Desai, Wenwen Lu and A.B. Tanner, "On the Long-Term Stability of Microwave Radiometers Using Noise Diodes for Calibration," *IEEE Trans. Geosci. Remote Sens.,* vol.45, no.7, pp.1908–1920, May 2007. http://dx.doi.org/10.1109/TGRS.2006.888098

[12] S. Misra and C.S. Ruf, "Detection of Radio-Frequency Interference for the Aquarius Radiometer," *IEEE Trans. Geosci. Remote Sens.,* vol.46, no.10, pp.3123–3128, Oct. 2008. http://dx.doi.org/10.1109/TGRS.2008.920371

[13] F.J. Wentz and D.M. LeVine, “Algorithm Theoretical Basis Document: Aquarius Salinity Retrieval Algorithm,” Remote Sensing Systems, Santa Rosa, CA, USA, RSS Technical Report 082912, 2012. [Online]. Available FTP: ftp://podaac-

ftp.jpl.nasa.gov/allData/aquarius/docs/v2/AQ-014-PS-0017_AquariusATBD_Level2.pdf

[14] J.R. Piepmeier, “Algorithm theoretical basis document for apparent aperture temperature, ” NASA’s Goddard Space Flight Center, Greenbelt, MD, USA, GSFC AQU-REF-001505, 2010. [Online]. Available: http://oceancolor.gsfc.nasa.gov/AQUARIUS/DOCS/AQU-REF-001505_comprehensive_ATBD_TAA.pdf

[15] J. Lilly and G. Lagerloef, “Aquarius Level 3 processing algorithm theoretical basis document. Version 0.9,” Earth and Space Research, Seattle, WA, USA, 2008. [Online]. Available FTP: ftp://podaac-ftp.jpl.nasa.gov/allData/aquarius/docs/v2/AquariusLevel3_GriddingSmoothingPaper_Lilly&Lagerloef2008.pdf

[16] J.R. Piepmeier, ed., “Aquarius Radiometer Post-Launch Calibration for Product Version 2,” NASA’s Goddard Space Flight Center, Greenbelt, MD, USA, AQ-014-PS-0015, 2013. [Online]. Available FTP: ftp://podaac-ftp.jpl.nasa.gov/allData/aquarius/docs/v2/AQ-014-PS-0015_AquariusInstrumentCalibratrionDescriptionDocument.pdf

[17] V.S. Reinhardt, Yi Chi Shih, P.A. Toth, S.C. Reynolds, A.L. Berman, "Methods for measuring the power linearity of microwave detectors for radiometric applications," *IEEE Trans. Microw. Theory Techn.*, vol.43, no.4, pp.715–720, Apr 1995. http://dx.doi.org/10.1109/22.375216

APPENDIX

The calibration algorithm includes a nonlinearity correction at the counts level before calibration coefficients are computed and applied:

$$p(h(T_{sys})) = gT_{sys}$$

where T_{sys} is the system noise temperature, $h(T_{sys})$ is the true (non-linear) transfer function of the radiometer, and $p(\cdot)$ is the linearizing function cast as polynomial:

$$p(x) = x + \sum_{i=2}^{n} c_i x^i$$

For Aquarius, a third order polynomial is used, which is consistent with expansive behavior of detectors and the compressive behavior of microwave amplifiers (e.g., [17]). Thus after radiometer counts are linearized, the gain of the resultant system is constant:

$$\frac{\partial}{\partial T_{sys}} p(h(T_{sys})) = g$$

Because the radiometer has internal noise diodes, which add a constant amount of power, the differential equation can be approximated as a finite-difference equation:

$$\frac{p(C_{ND,j}) - p(C_j)}{T_{ND}} = g$$

where C_j are antenna counts for the j^{th} value of T_{sys} and $C_{ND,j}$ are antenna plus noise diode counts. The difference in counts caused by turning on the noise diode is the so-called noise diode deflection. The product of noise diode temperature and linear gain equals the linearized deflection and the above can be rewritten as a deflection ratio:

$$\frac{p(C_{ND,j}) - p(C_j)}{p(C_{ND,0}) - p(C_0)} = 1$$

For convenience, gT_{ND} is defined at some reference value of T_{sys} denoted by the subscript-0, which here is at the minimum antenna temperature. Given a number of observations j of noise diode deflections for different input system temperatures, the coefficients of p can be found by solving an overdetermined linear system of equations:

$$[C_j - C_{ND,j} - C_0 + C_{ND,0}]_{j,1} = [C_0^i - C_j^i - C_{ND,0}^i + C_{ND,j}^i]_{j,i}[c_i]_{i,1}$$